ADVANCED ELECTRONIC MATERIALS Open Access
www.advelectronicmat.de

Interplay of Backbone Conformation, Morphology and Thermoelectric Properties of Benzodifuranone-Isatin Acceptor Polymers

*Diego R. Hinojosa, Nathan J. Pataki, Francesca Pallini, Guillaume Freychet, Andreas Erhardt, Kevin Schuller, Selina Olthof, Klaus Meerholz, Christopher R. McNeill, Mario Caironi, Florian Günther, and Michael Sommer**

Benzodifuranone (BDF)-isatin-based conjugated acceptor copolymers with different stereoelectronic properties are designed, guided by density functional theory calculations. *syn*- and *anti*-conformations are predicted to depend on both the presence of chlorine substituents as well as on the steric demand of the comonomer. Backbone torsion decreases with the comonomer of the order thiophene (T) > furan (F) > acetylene (A). Six copolymers of BDF-isatin with T, F, and A are prepared, referred to as H-BDF-T, Cl-BDF-T, H-BDF-F, Cl-BDF-F, H-BDF-A, and Cl-BDF-A. Electrochemically and spectroscopically determined HOMO and LUMO energy levels align qualitatively and confirm a stabilization of the LUMO of the chlorinated copolymers. The thin film microstructures of H-BDF-A and Cl-BDF-A, having a linear backbone, are characterized by an edge-on orientation, while the four remaining copolymers with a more curved backbone predominantly orient face-on. The non-chlorinated furan copolymer H-BDF-F stands out due to its curved yet coplanar backbone, face-on orientation, high degree of crystallinity, close $\pi-\pi$ stacking distance, the highest electrical conductivity of 3 S cm^{-1}, the best air stability of electrical conductivity among the series, and an appreciably high power factor. These results demonstrate that theory-guided design allows for optimizing nonhalogenated n-type copolymers of low synthetic complexity for thermoelectric applications.

1. Introduction

Conjugated polymers (CPs) comprise aromatic units, double or triple bonds brought into conjugation, thus creating a delocalized π−system along the backbone.[1] This electronic interaction is the basis for unique optoelectronic properties, including charge mobility and optical absorption. CPs have found applications in different technological areas such as organic light emitting diodes (OLEDs),[2,3] organic field effect transistors (OFETs),[4–6] organic photovoltaics (OPVs),[7,8] and organic thermoelectrics (OTEs).[9,10] The chemical structure of CPs is widely tunable, which offers tailoring of properties. CPs show semiconducting behavior in their pristine, undoped form, hence, charge carrier injection is necessary to render them conductive, except for some exceptions.[11–13] Depending on their electronic nature, CPs can be classified

D. R. Hinojosa, M. Sommer
Technische Universität Chemnitz
Institut für Chemie
Straße der Nationen 62, 09111 Chemnitz, Germany
E-mail: michael.sommer@chemie.tu-chemnitz.de
D. R. Hinojosa, M. Sommer
Forschungszentrum MAIN
Rosenbergstraße 6, 09126 TU Chemnitz, Germany
N. J. Pataki
Department of Physics
Politecnico di Milano
Pizza Leonardo da Vinci 32, Milano 20133, Italy
The ORCID identification number(s) for the author(s) of this article can be found under https://doi.org/10.1002/aelm.202500213

DOI: 10.1002/aelm.202500213

N. J. Pataki, M. Caironi
Center for Nano Science and Technology
Via Rubattino 81, Milan 20134, Italy
F. Pallini
Department of Materials Science
Università di Milano-Bicocca
via Cozzi 55, Milan 20125, Italy
G. Freychet
Univ. Grenoble Alpes
CEA
Leti
Grenoble F-38000, France
A. Erhardt, C. R. McNeill
Department of Materials Science and Engineering
Monash University
Clayton, Victoria 3800, Australia
S. Olthof
Chair for Surface and Material Analysis
University of Wuppertal
Rainer-Gruenter-Str. 21, 42119 Wuppertal, Germany

into *p*-type and *n*-type materials. *p*-type CPs are rich in electron density and commonly based on sulfur-containing heterocycles such as thiophene,[14] thienothiophene,[15] or bithiophene.[16] This leads to macromolecules with high-lying highest occupied molecular orbitals (HOMOs) resulting in relatively easy (electro)chemical oxidation. *n*-type CPs require the presence of electron-deficient functional groups such as lactones, lactams, halogens, or nitrile groups to effectively lower the lowest unoccupied molecular orbital (LUMO) energy level and favor electron injection processes.[17–20]

The use of conjugated polymers as thermoelectric materials is an attractive alternative compared to inorganic semiconductors.[21,22] Thermoelectric materials have the potential to transform waste heat into electricity via the Seebeck effect. To quantify the performance of thermoelectric materials, the dimensionless figure of merit $zT = S^2\sigma Tk^{-1}$ is used. Here, S is the Seebeck coefficient, σ is the electrical conductivity, T is the temperature, and k is the thermal conductivity. Since the thermal conductivity is low and dominated by phonons at typical doping levels,[23] the power factor, defined as $PF = S^2\sigma$, is often employed to determine the performance of a thermoelectric material. Electrical conductivity is given by $\sigma = \mu_e n_e e$, and thus the product of the mobility μ_e, the charge carriers concentration n_e, and the elementary charge e. CPs need external charge carrier injection, i.e., sub-stoichiometric oxidation or reduction, to achieve a high σ that in turn allows for increasing the PF. As S usually decreases with an increasing charge carrier density at the same time, an experimental modulation of the charge carrier density is required to maximize the PF. A common way of achieving this is via chemical doping.[24] For *p*- and *n*-doping, an external oxidant and reducing agent are added, respectively.[25,26] As a result, radical cations and radical anions, respectively, form on the polymer backbone. It is critical to optimize the LUMO level of *n*-type materials, since its position determines the stability and potential re-oxidation of the radical anion to the neutral state in the presence of oxygen, an aspect that in turn allows for the processing and operation of thermoelectric modules under ambient conditions.[27]

Recently, the oxidative homopolymerization of benzodifuranone (BDF) was shown to furnish a self-doped CP with high conductivity and ambient stability of the resulting radical anions due to an extremely low-lying LUMO level of −5.18 eV.[28] While molecular doping is a complex process involving diverse aspects,[29,30] the HOMO and LUMO energy levels of both the polymer (host) as well as the dopant are key variables, in addition to dopant-polymer miscibility[31–33] and processing.[34,35] Especially important is the role of the polymer side chains, with mixed polar/alkyl side chains being particularly promising.[36] Implementation of such amphiphilic structure into a diketopyrrolopyrrole-based polymer has led to a high zT value of 0.46.[37] Rigid and coplanar backbones with fused motifs and non-covalent conformational locks are important to achieve high charge carrier mobilities, making them common design motifs also for organic thermoelectric materials.[17,38] Furthermore, a detailed study on the effect of backbone curvature of isoindigo-based CPs indicated that centrosymmetric donors led to larger field-effect hole mobilities compared to axisymmetric analogs.[39] This result was explained by a more linear backbone and enhanced π–π stacking, order, and thus improved charge transport. Yang Lu et al. further demonstrated that backbone symmetry has a major influence on performance. In a series of thienoisatin-benzodifuranone copolymers, linear backbones led to better ordering and lower electrical conductivity upon n-doping.[40] However, while these structure-relationships have proven insightful, a better understanding of the combined effects of different conformations, energy levels, morphology, and performance of n-type CPs used for thermoelectric applications is still needed. Moreover, with the synthetic complexity of many n-type CPs being relatively large, simpler structures prepared by straightforward protocols are required. Previously, we have designed a simple side chain that provides high solubility for strongly aggregating n-type CPs and showed that the resulting larger molar masses could improve the electrical conductivity upon n-doping.[41]

In this work, we design and synthesize synthetically simple, isatin-flanked BDF monomers with varying LUMO levels and link them with varying comonomers such that backbone conformation and curvature, thin film morphology, and the resulting thermoelectric properties are altered. Two major handles are exploited to modulate chemical structure. While the comonomer mostly influences backbone curvature, substitution of the BDF-flanking isatin with chlorine allows for lowering the LUMO energy level by ≈0.2 eV.[18] The different comonomers thiophene (T), furan (F), and acetylene (A) were selected on the basis of density functional theory (DFT)-predicted torsion potentials that allow to modulate *syn*- and *anti*-conformations, backbone coplanarity, and curvature. Using a broad set of experimental characterization tools, including ultraviolet photoelectron spectroscopy (UPS), inverse photoelectron spectroscopy (IPES), grazing incidence wide-angle X-ray scattering (GIWAXS), thermoelectric characterization, and electrical conductivities under ambient conditions, we show how stereoelectronic factors influence backbone curvature and thus orientation in thin films. While curved backbones tend to orient face-on, linear ones adopt an edge-on orientation. The combined effects of backbone curvature and the resulting orientation, as well as backbone coplanarity and the resulting crystallinity, strongly influence electrical conductivity and finally thermoelectric performance. We find that a combination of slightly curved backbones, face-on orientation, and improved crystallinity is most beneficial for improving the electrical conductivity and the power factor of doped films.

2. Results and Discussion

2.1. Theory-Guided Design of Isatin-Flanked BDF Copolymers

DFT calculations were performed to guide the design of different BDF-isatin copolymers. Chlorination was first considered as

K. Schuller, S. Olthof, K. Meerholz
Department of Chemistry
University of Cologne
Greinstrasse 4–6, 50939 Cologne, Germany
F. Günther
São Paulo State University (UNESP)
Instituto de Geociências e Ciências Exatas (IGCE)
Campus Rio Claro
Rio Claro – SP 13506–700, Brazil

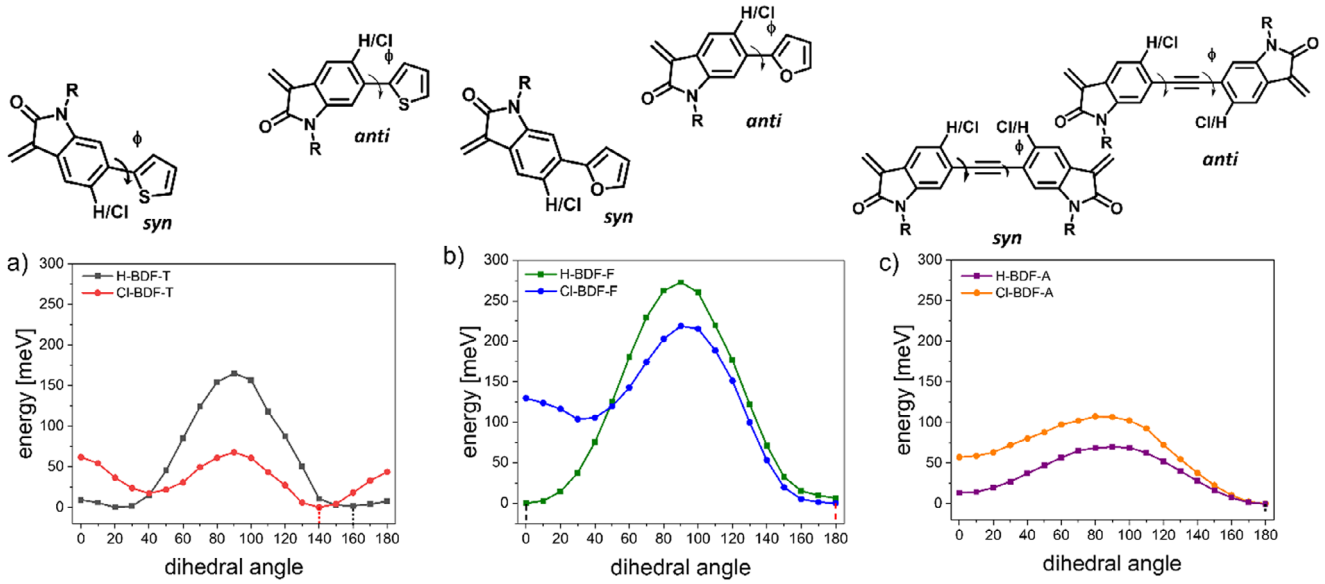

Scheme 1. Torsional energies of a) isatin-thiophene, b) isatin-furan, and c) isatin-acetylene-isatin models as obtained from DFT/PBE/DZVP calculations for non-chlorinated (black) and chlorinated (red) isatin units. Dashed vertical lines indicate the minima. Note that the abbreviations of the polymers are used in the legend, although the actual molecules calculated are models with chemical structures shown at the top of this scheme.

a structural modification to lower the LUMO level due to its electron-withdrawing nature and straightforward synthetic implementation. As comonomers, T, F, and A were chosen based on their simplicity, overall small size that minimizes steric hindrance with the neighboring isatin motif, as well as commercial availability of the corresponding stannylated forms required for Stille cross-coupling. F is smaller than T due to the shorter C—O bond and therefore was anticipated to allow for a greater extent of coplanarity.[42] However, both T and F would lead to curved backbones due to their five-membered ring structure. Using A as the comonomer allows for to formation of fully linear backbones and coplanarity at the same time. In order to estimate linearity and coplanarity of the backbone, models of the repeat unit terminated by hydrogen atoms and side chains substituted by methyl groups were optimized. For all models, torsion angles of about 11° between the isatin and BDF units were observed, causing bent backbones (Figure S1, Supporting Information). This result agrees with a report by Lei et al.[43] who found an angle of 7.6° from B3LYP/ 6–311+G(d,p) calculations. Chlorination and comonomer variation barely affected the geometry of the BDF acceptor units, except for small variations within the certainty of the utilized method. However, the presence of chlorine combined with the different sizes of T, F, or A strongly influenced the isatin-comonomer dihedral angle. Thus, H-BDF-T showed a residual dihedral angle of 7.3°, which increased to 32° for Cl-BDF-T. The F-based copolymers H-BDF-F and Cl-BDF-F were mostly coplanar with torsion angles < 0.5° in both cases. This is due to the fact that the oxygen-carbon bond length is shorter than the sulfur-carbon bond length, rendering F significantly less sterically demanding.

In all cases, HOMO-LUMO gaps of ≈1.0 eV were obtained irrespective of any model modification. In all cases, the frontier orbitals were lowered by ≈0.2 eV upon chlorination, confirming the H / Cl exchange as a valid strategy to enhance the electron-withdrawing properties of the systems. To further assess the structural properties of the different systems, the rotation potentials of successive units were studied by considering two-unit models (**Scheme 1**). In these models, the dihedral angle was fixed, while all remaining degrees of freedom were relaxed. The isatin units were terminated with *exo*-methylene groups to represent the double bond to the BDF unit. The rotational energy for the H-BDF-T model is shown in Scheme 1a (gray curve). It shows that *syn*- and *anti*-conformations exhibit similar energies and a dihedral angle of ≈15°, with barriers for full coplanarity of ≈10 meV. Upon exchanging H by Cl (Scheme 1a, red curve), the dihedral angle increases to ≈40° for both *syn*- and *anti*-conformations. Associated barriers to full coplanarity rise to ≈40 meV due to the higher steric demand of chlorine. Moreover, the minimum of the *syn*-orientation is ≈20 meV higher in energy and therefore less favorable. It is interesting to note that, due to the steric hindrance between thiophene and chlorine, the rotation barrier at 90° decreased from 160 to 60 meV. This would support an energetically favored switch from *syn*- to *anti*-conformation of Cl-BDF-T. When T is replaced by F (Scheme 1b), the *syn*- and *anti*-conformation of H-BDF-F are again energetically similar, but this time backbones are fully coplanar. Upon H / Cl exchange, however, the *syn*-orientation becomes nonplanar with a dihedral angle of ≈30° and energetically unfavored due to a relative difference of 100 meV compared to the *anti*-conformation, which remains coplanar. For the model with A as donor, full coplanarity between successive isatin units is found for both *syn*- and *anti*-conformers of H-BDF-A and Cl-BDF-A (Scheme 1c). However, the *syn*- and *anti*-conformers differ in their energies, with the *anti*-conformers being favored by ≈20 meV in the case of H-BDF-A and by ≈60 meV in the case of Cl-BDF-A compared to the corresponding *syn*-conformers. The two conformers are further separated by a rotational barrier of 68 and 114 meV for H-BDF-A and Cl-BDF-A, respectively.

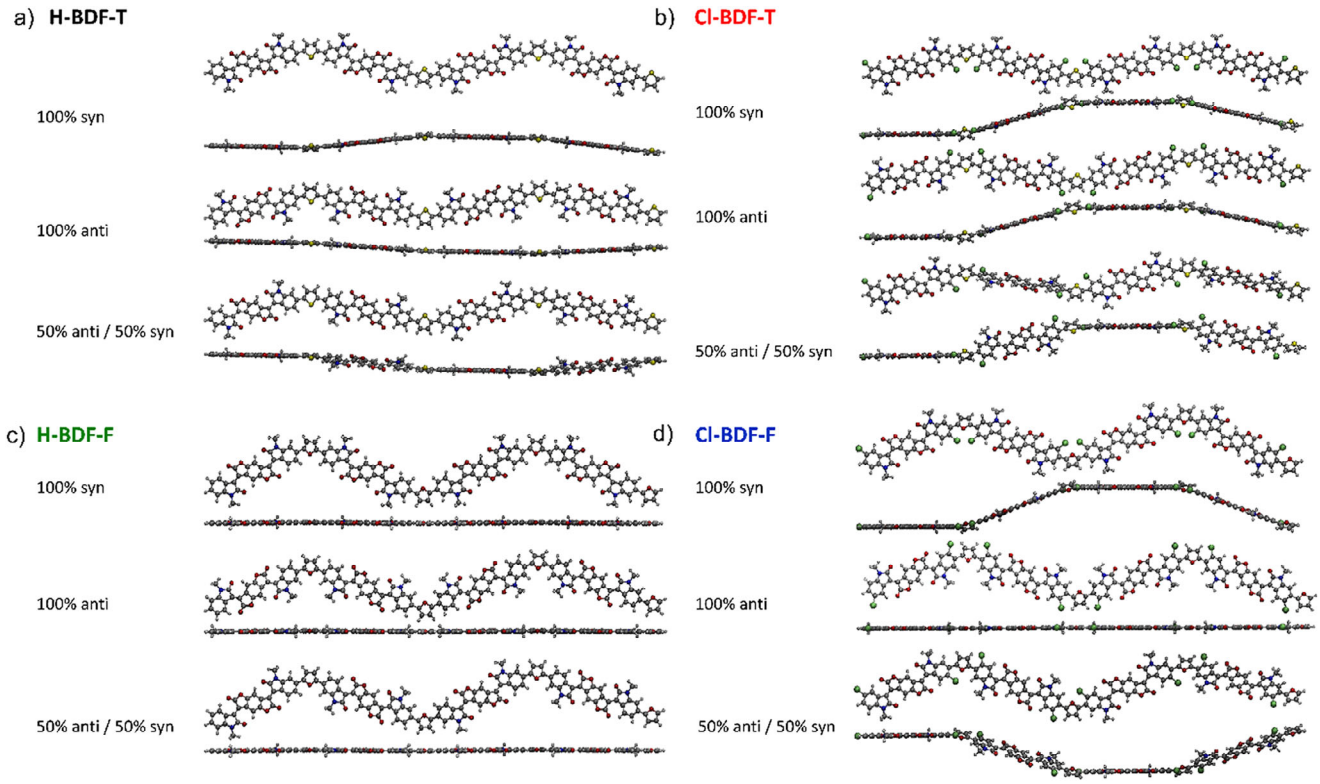

Scheme 2. Geometry-optimized structures of BDF-isatin model tetramers with a), b) thiophene and c), d) furan as comonomer.

We also studied the rotational barriers around the double bond between isatin and BDF units (Figure S2, Supporting Information). As expected, a large barrier of >500 meV is found, associated with the breaking of the double. Furthermore, the orientation in which both carbonyl groups point toward each other results in a nonplanar and much less favored structure with an energy difference of 360 meV compared to the opposite direction. The energetically most favored configuration is found for a twist of about 10°.[43] The barrier to the fully coplanar structure is only ≈5 meV and therefore much smaller than the thermal energy at room temperature ($k_BT \approx 23$ meV) or the energy gain due to π–π stacking (> 100 meV). It can therefore be concluded that BDF-isatin units tend to full coplanarity in the solid state.

To consider how Cl substitution and the geometry of the curved backbones with five-membered comonomers T and F affect long-range structural arrangement, models featuring several repeat units were generated (**Scheme 2**). The angle between the two sides of the different donor units induces kinks into the backbone structures. As shown in Scheme 2, this effect is strongest for F (Scheme 2c,d) and weaker for T (Scheme 2a,b). Two successive *syn*-conformations for F and T cause a stronger backbone curvature. Furthermore, two successive *anti*-conformations bring the solubilizing side chains closer to each other, resulting in additional steric hindrance. Considering these contributions, a backbone conformation of alternating *syn*- and *anti*-conformations, where the side chains of successive units point into opposite directions, is optimal for improving crystallinity (Scheme 2c). Since H-BDF-F exhibits the highest degree of coplanarity and similar preferences for *syn*- and *anti*-conformations, improved packing and crystallinity in comparison to T analogs are expected.

2.2. Synthesis and Characterization of BDF Polymers

With the results from DFT calculations in hand, a synthetic route was designed for all copolymers. Chlorination was achieved via electrophilic aromatic chlorination of commercially available 6-bromoisatin **1a** using sulfuryl chloride, furnishing 5-chloro-6-bromoisatin **1b** (**Scheme 3a**).[18] N-Alkylation of the isatin with single-oxygen side chains proceeded in a dimethylformamide (DMF) / tetrahydrofuran (THF) mixture to yield **2a-b**.[41] The monomers were finally obtained via acid-catalyzed aldol condensation of **2a-b** with BDF to give **3a-b** (Scheme 3b). All intermediates and products were thoroughly characterized by nuclear magnetic resonance (NMR) spectroscopy (Figures S3–S22, Supporting Information). All polymers were synthesized from **3a** or **3b** and distannylated T, F, and A via Stille polymerization at 100 °C in toluene as described in the Supporting Information (Scheme 3c). The crude mixtures were precipitated into methanol and purified via Soxhlet extraction, furnishing yields between 60% to 90%. A summary of the molecular properties of the different polymers is compiled in **Table 1**. The relative molecular weights of all polymers were determined using high-temperature size exclusion chromatography (SEC) in 1,2,4-trichlorobenzene at 120 °C (Figure S23, Supporting Information). The T copolymers H-BDF-T and Cl-BDF-T exhibited the highest number average molecular weights (M_n), likely as a result of the increased reactivity of

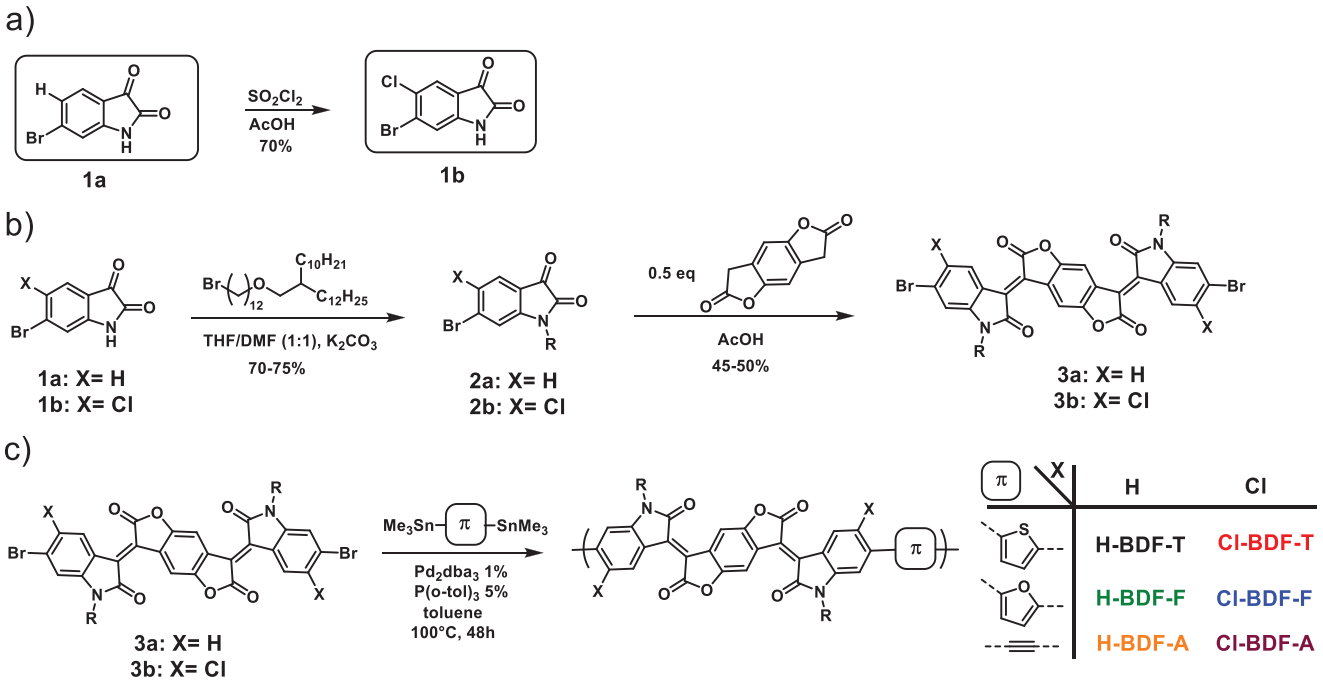

Scheme 3. Synthesis of BDF/ isatin-based copolymers used in this study. a) Chlorination of 6-bromoisatin **1a**. b) Synthesis of BDF comonomers **3a-b**. c) Synthesis of polymers H-BDF-T, Cl-BDF-T, H-BDF-F, Cl-BDF-F, H-BDF-A and Cl-BDF-A.

the T comonomer, which is thought to facilitate the rate-limiting transmetalation step.[44] The F-based copolymers H-BDF-F and Cl-BDF-F displayed the lowest yields, which is attributed to the difficulty in handling the liquid distannylated F, rendering precise control over stoichiometry more challenging. M_n values of the A copolymers H-BDF-A and Cl-BDF-A were lowest as a result of the limited purity of commercial A of only ≈97%. Considering the linearity and therefore higher rigidity of the copolymers with A, the obtained relatively low molecular weights may be influenced by a stronger degree of overestimation of molecular weight compared to the remaining four examples. As a result, the difference in absolute number average molecular weights between the A copolymers and the remaining ones may be even larger.

2.3. Optoelectronic Properties

The optical properties of the polymers were investigated via UV–vis spectroscopy in 1,2-orthodichlorobenzene (*o*-DCB) (**Figure 1**).

Table 1. Summary of molecular properties of BDF-isatin copolymers.

Polymer	M_n[a)] [kg mol^{-1}]	M_w[a)] [kg mol^{-1}]	$Đ$[a)]	Yield %
H-BDF-T	55	143	2.6	98
Cl-BDF-T	47	104	2.2	82
H-BDF-F	20	24	1.2	60
Cl-BDF-F	35	77	2.2	75
H-BDF-A	18	40	2.2	75
Cl-BDF-A	18	41	2.3	97

[a)] determined by size exclusion chromatography in 1,2,4-trichlorobenzene at 120 °C and calibrated with polystyrene standards.

The two copolymers H-BDF-T and Cl-BDF-T with T showed similar absorption profiles. For H-BDF-T, two vibronic transitions *0–1* and *0-0* appeared at 750 and 814 nm, respectively.[45,46] Cl-BDF-T shows a slight hypsochromic shift of ≈20 nm to 730 nm and 795 nm, which is attributed to the increased dihedral angle caused by the bulkier chlorine atom. According to the results from DFT calculations, the rotational potential of Cl-BDF-T exhibits two minima, whereby the energy of the *anti*-conformation is lower in energy (Scheme 1a). The F-based copolymers showed a qualitatively reversed trend upon chlorination compared to the copolymers with T. H-BDF-F exhibited a blueshifted onset of absorption compared to Cl-BDF-F, likely as a result of the increased coplanarity of the F-based copolymers that allows the stronger acceptor unit BDF-Cl to come into effect. The vibronic bands of H-BDF-F and Cl-BDF-F were generally less developed compared to the T-based copolymers, however, both for copolymers with T and F, chlorination led to a more intense *0-0* transition. The trends of relative intensities of *0–0* and *0–1* transitions were also seen in the corresponding thin film absorption spectra, indicating that local chain packing in aggregates in solution and in thin films is similar. The two copolymers with A exhibited hypsochromically shifted spectra compared to the other four copolymers. H-BDF-A showed significantly better resolved vibronic transitions at 690 and 748 nm, with the latter being the most intense vibronic band. The non-chlorinated Cl-BDF-A showed a featureless spectrum with a much less steep onset of absorption.

To further investigate the nature of aggregates, temperature-dependent absorption spectra were recorded in *o*-dichlorobenzene between 30 and 150 °C (Figures S24–S26, Supporting Information). In all cases, we assume that aggregation is strong and that aggregates are not fully dissolved within the experimentally accessible conditions. The reduced intensity

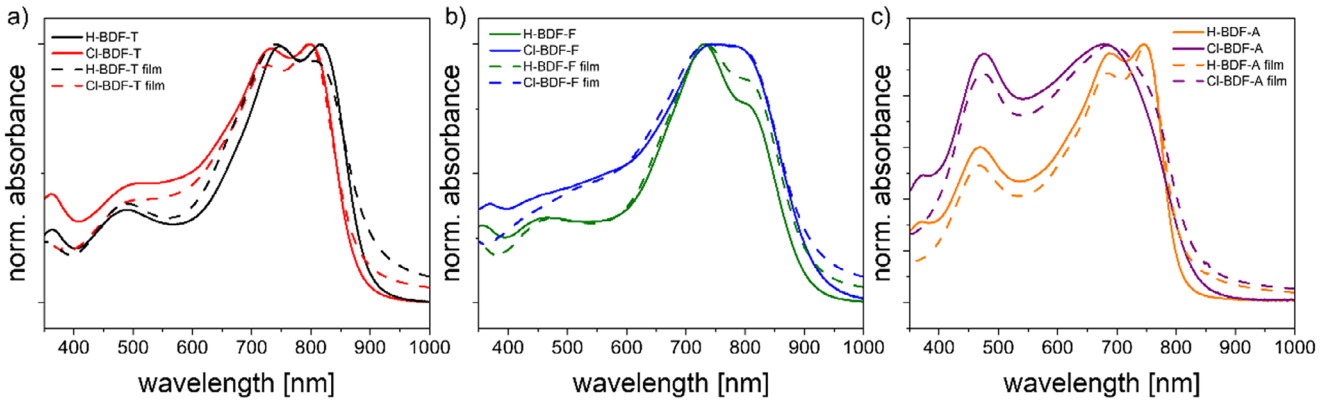

Figure 1. UV–vis spectra of polymers in solution (solid lines) and in film (dashed lines). a) H-BDF-T and Cl-BDF-T, b) H-BDF-F and Cl-BDF-F and c) H-BDF-A and Cl-BDF-A. Solution spectra were taken in *o*-DCB at 0.02 mg mL^{-1}.

of the *0-0* transition of H-BDF-T, Cl-BDF-T, and H-BDF-A upon heating indicates J-aggregation-dominated behaviour.[47] The changes in the temperature-dependent spectra of the F copolymers and Cl-BDF-A are qualitatively similar, but due to their less defined vibronic transitions an identification of the H- and J-type terminology is not clear.

The energy levels were determined using two different methods, given the importance of the position of the LUMO energy level for the stability of negative polarons (radical anions) under ambient conditions. Cyclic voltammetry (CV) in film was measured by drop casting films from chloroform and acquiring CV cycles in a 0.1 M tetrabutylammonium hexafluorophosphate solution in acetonitrile. The electrochemical redox potentials (onset method) versus ferrocene/ ferrocenium are given in **Table 2** with −4.8 eV as the reference potential of Fc/Fc^+ oxidation.[48] The LUMO levels of the three chlorinated polymers were lower by ≈0.1–0.2 eV compared to non-chlorinated analogs (**Figure 2**, for CV curves see Figures S27–S29, Supporting Information). While all polymers exhibited good stability during multiple electrochemical reduction cycles, they were unstable under positive potentials and decomposed when subjected to more oxidizing conditions.

In addition to the CV, the energy levels were estimated spectroscopically from ultraviolet photon spectroscopy (UPS) and inverse photoelectron spectroscopy (IPES). The spectra are shown in Figure S30 (Supporting Information), while the extracted values for the HOMO and LUMO position are included in Table 2. Compared to the CV data, the HOMOs of different copolymers measured by UPS are found to be up to 0.4 eV more negative, as can be seen in Figure 2. This shift is likely related to the presence of the solvent and the electrolyte $TBAPF_6$ in the CV measurement, which affects the dielectric constant of the film and leads to better screening of the charge carriers in the case of CV. For the same reason, the LUMO levels are up to 0.3 eV higher. The only exception is H-BDF-F, where both HOMO and LUMO are further upshifted relative to CV than the other compounds. This is likely related to surface contamination, as traces of Si of unknown origin were observed in an XPS measurement (data not shown), which did affect the readout of the work function. As displayed in Figure S30 (Supporting Information), the work function is distinctly different for this sample compared to the others. Due to the changed environment, the UPS/IPES bandgap is measured to be 0.3 to 0.6 eV higher than the one determined by CV, but overall, the trends in HOMO and LUMO positions are nonetheless the same as summarized in Figure 2, meaning that chlorination lowers the LUMO levels.

2.4. Conductivity and Thermoelectric Performance of BDF Polymers

To investigate the electrical conductivity, the polymers were doped using 4-(1,3-dimethyl-2,3-dihydro-1H-benzoimidazol-2-yl)-N,N-dimethylaniline (N-DMBI) via coprocessing, i.e., dissolv-

Table 2. Summary of energy levels of BDF-isatin copolymers.

Polymer	Reduction/ oxidation onset potential vs Fc/Fc^+ [V]	HOMO/LUMO from CV[a)] [eV]	HOMO/LUMO from UPS/ IPES [eV]	HOMO/LUMO Theory[b)] [eV]	E_g^{EC} [eV]	E_g^{UPS} [eV]	E_g^{opt} [eV]
H-BDF-T	0.23/−0.80	−5.40/4.02	−5.62/3.83	−5.21/-4.16	1.38	1.79	1.38
Cl-BDF-T	0.26/−0.60	−5.46/−4.22	−5.79/3.93	−5.40/−4.38	1.24	1.86	1.40
H-BDF-F	0.28/−0.71	−5.48/−4.11	−5.44/−3.68	−5.44/−3.68	1.37	1.76	1.37
Cl-BDF-F	0.36/−0.60	−5.57/−4.22	−5.72/−4.07	−5.34/−4.35	1.35	1.65	1.35
H-BDF-A	0.47/−0.67	−5.68/−4.15	−5.89/3.96	−5.38/−4.29	1.53	1.93	1.55
Cl-BDF-A	0.49/−0.60	−5.70/−4.22	−5.94/−4.02	−5.54/−4.11	1.48	1.92	1.45

[a)] −4.8 eV as a reference; [b)] values obtained from DFT/PBE/DZP.

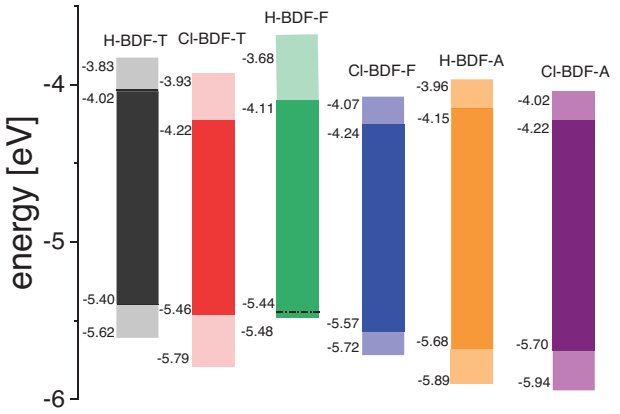

Figure 2. HOMO and LUMO bandgaps of polymers determined by cyclic voltammetry (smaller gaps) and UPS/IPES (larger gaps); see also Table 2.

ing the dopant and the polymer in toluene and preparing samples by spin coating the obtained solution in a N_2-filled glovebox. UV–vis spectroscopy was used to confirm doping of the thin films as observed by the bleaching of the neutral band and growth of the polaronic bands (Figure S31, Supporting Information). The electrical conductivity of the doped films was measured as a function of the molar ratio (% MR) of the dopant relative to the polymer repeat unit, ranging between 20%–70% (**Figure 3**).

A broad range of conductivities between 10^{-5} to 10^{0} S cm^{-1} was found. The highest conductivities obtained were between 0.1–3 S cm^{-1} for H-BDF-T, Cl-BDF-T, and H-BDF-F. The highest value of 3 S cm^{-1} was observed for H-BDF-F at 60% MR doping. Polymers with lower maximum conductivity (e.g., H-BDF-A and Cl-BDF-A) reached their peak at 30–40 MR% dopant concentration, while those with higher maximum conductivity (e.g., Cl-BDF-T and H-BDF-F) peaked at 50–60 MR%. It is interesting to note that the performance in terms of conductivity and Seebeck coefficients is very similar for the two T copolymers, H-BDF-T and Cl-BDF-T, irrespective of H/ Cl exchange, whereas the performance between the two F copolymers, H-BDF-F and Cl-BDF-F, is strikingly different. Here, the presence of chlorine appeared to be deleterious to the electrical conductivity, as the σ_{max} achieved by this polymer remained below 0.1 S cm^{-1}, more than an order of magnitude lower than the σ_{max} of 3 S cm^{-1} achieved by the non-chlorinated H-BDF-F. A more drastic effect of the dopant concentration could be observed for the polymers containing acetylene as comonomer, H-BDF-A and Cl-BDF-A. In these cases, the σ_{max} was reached at a much lower doping concentration of 30% MR, after which a strong drop in the electrical conductivity was observed between 30% MR and 70% MR. In comparison to the whole series, the A copolymers exhibited very low electrical conductivities and were not considered for further characterization. One possible cause is their low molecular weight, which has been identified as a limiting factor for the conductivity.[41] The conductivity of H-BDF-F is, to the best of our knowledge, the highest reported for BDF-isatin flanked, non-halogenated systems doped with N-DMBI.[18]

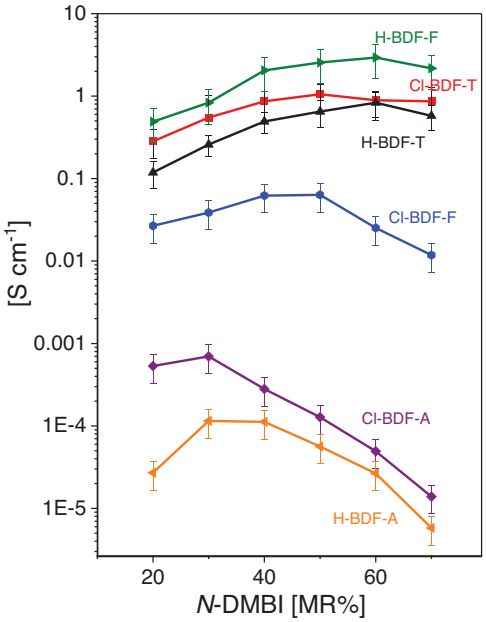

Figure 3. Electrical conductivity of co-processed thin films of H-BDF-T, Cl-BDF-T, H-BDF-F and Cl-BDF-F, H-BDF-A, and Cl-BDF-A as a function of the N-DMBI dopant concentration. Error bars for electrical conductivity values arise from the experimental error of the film thickness measurement and do not represent a standard deviation.

The Seebeck coefficients (S) of the polymers H-BDF-T, Cl-BDF-T, H-BDF-F, and Cl-BDF-F were also measured, enabling the calculation of the power factors PF = σS^2 (**Figure 4**). As expected, the highest values of Seebeck coefficients were recorded at the lowest % MR in all cases where the carrier concentration is lowest, with Cl-BDF-F showing the highest value of S = −147 μV K^{-1}. In all cases, the absolute value of the Seebeck coefficient diminished with the increasing MR% of *N*-DMBI and increasing carrier concentration, in good agreement with the trends found in the literature.[49] Cl-BDF-T showed the highest PF of 0.20 μW m^{-1} K^{-2}, which is close to H-BDF-F, exhibiting the second highest one of 0.14 μW m^{-1} K^{-2}.

To further evaluate the effect of the LUMO energy level on the stability of electrical conductivity under ambient conditions (room temperature, humidity not controlled or monitored), the electrical conductivity was monitored under ambient conditions (**Figure 5**). The three samples H-BDF-T, Cl-BDF-T, and H-BDF-F were selected because of their highest conductivity and their varied LUMO energy level. In all cases, the conductivity decreased by one to two orders of magnitude after 100 to 1000 min. However, clear differences were evident among the three samples. First, the decrease in conductivity of Cl-BDF-T was less pronounced compared to H-BDF-T, confirming that the stabilization of the LUMO level of 0.2 eV is beneficial for enhancing the stability of radical anions under ambient conditions. While we note that the value of −4.22 eV for Cl-BDF-T obtained from CV is still not sufficiently low for a thermodynamic stability of a radical anion, kinetic stabilization may be achieved upon further reduction of the LUMO energy level beyond −4.0 eV.[27,50,51] Second, H-BDF-F exhibited the least degradation of conductivity despite its slightly more positive LUMO of −4.11 eV compared to Cl-BDF-T. A tentative explanation for this result can be found in its improved crystallinity (vide infra, 2.5 Packing and morphology) that

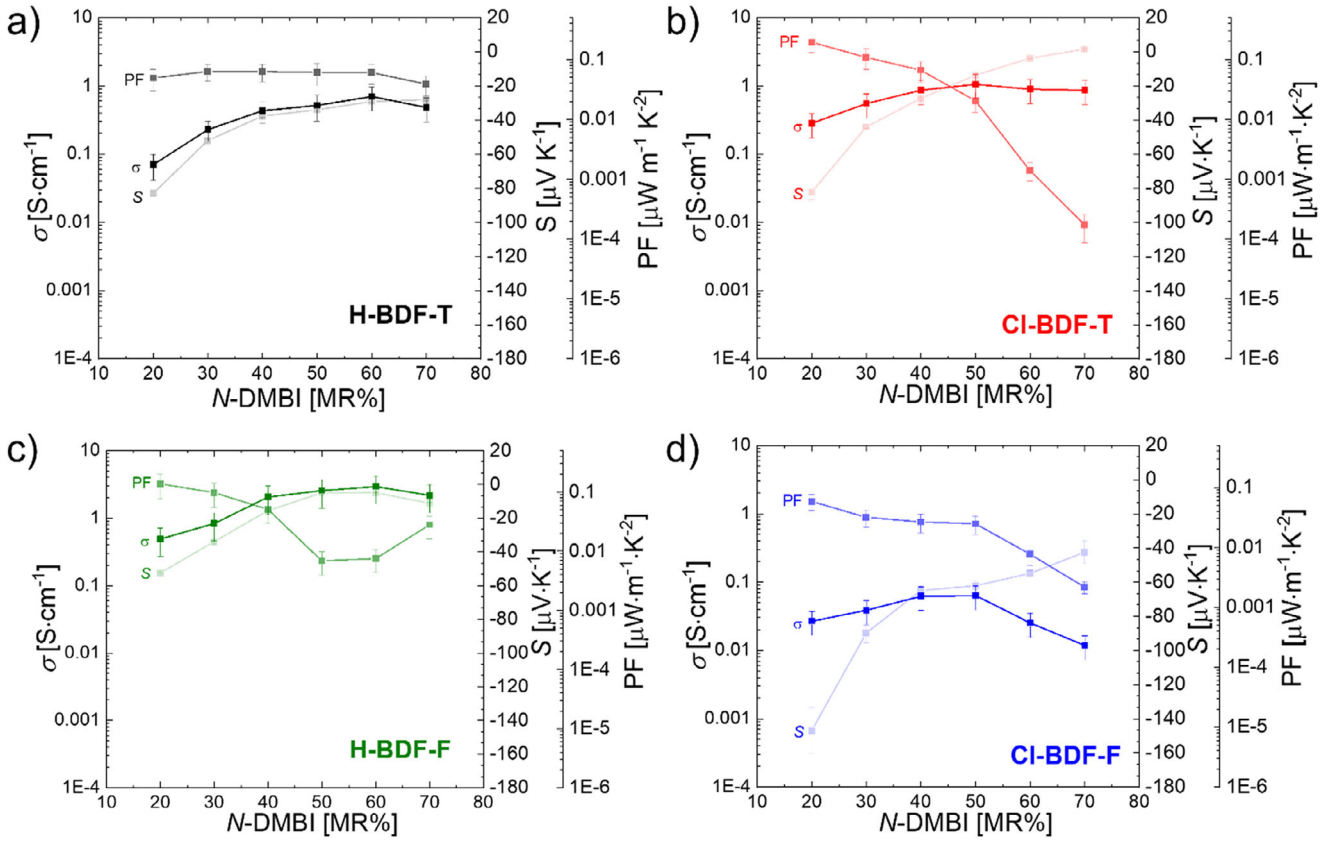

Figure 4. Electrical conductivities, Seebeck coefficients (S), and power factors (PF) of thin films of a) H-BDF-T, b) Cl-BDF-T, c) H-BDF-F, and d) Cl-BDF-F versus N-DMBI dopant concentration.

potentially slows down oxygen diffusion within the film, resulting in a morphological barrier. Proof of such a hypothesis is beyond the scope of this work, however, we note that similar correlations have been drawn for optically excited states in conjugated polymers of varying degrees of crystallinity.[52] Overall, we conclude that a beneficial combination of a stabilized LUMO energy level and degree of crystallinity may be a suitable strategy to improve kinetic stabilization of radical anions when thermodynamic stability is not possible for reasons related to chemical structure.

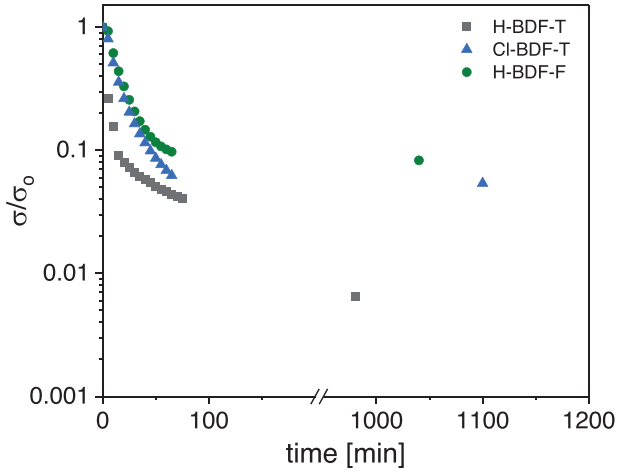

Figure 5. Electrical conductivities of H-BDF-T, Cl-BDF-T, and H-BDF-F under ambient conditions at 60% MR N-DMBI dopant concentration.

2.5. Packing and Morphology

The morphology of thin films was investigated using grazing incidence wide-angle X-ray scattering (GIWAXS). **Figure 6** presents GIWAXS patterns of neat films. All polymers exhibit a semicrystalline microstructure with well-defined main chain side chain separations and π–π stacking peaks. A key distinction amongst the polymers is that the A copolymers H-BDF-A and Cl-BDF-A exhibited an edge-on orientation of crystallites with side chain stacking out-of-plane and π–π stacking direction in-plane, while the T- and F-containing copolymers all exhibited a face-on orientation of crystallites. A possible reason for the significant difference in crystallite orientation is the geometry of the comonomer and the resulting degree of linearity of the backbone. We propose that the edge-on orientation of the fully linear A-based copolymers is one central cause for their very low conductivity. Linear chains may also accommodate less dopant molecules compared to curved backbones, an explanation that is corroborated by the peak in electrical conductivity at lower MR. Such trends for backbone linearity/ morphology/ conductivity relations can be

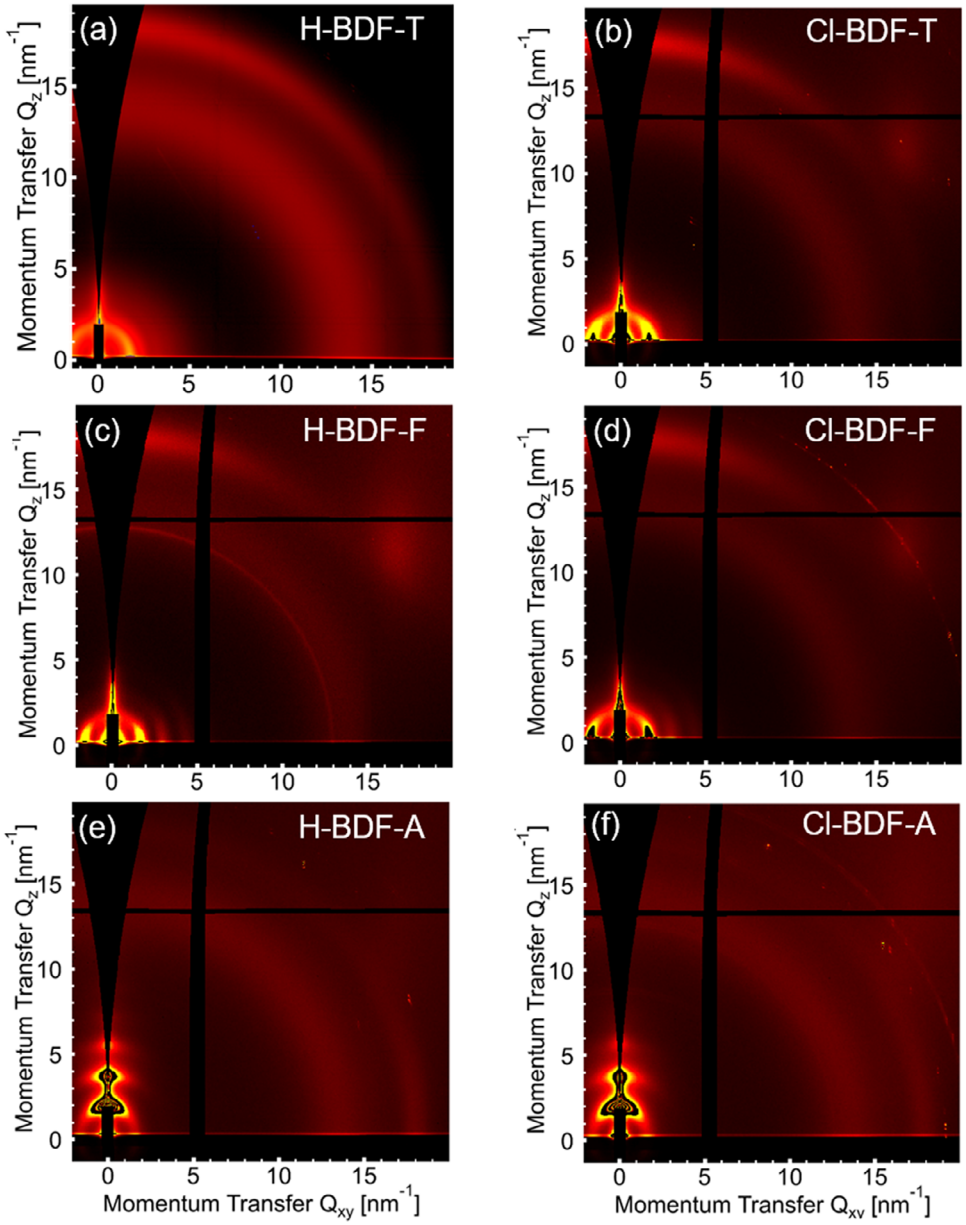

Figure 6. GIWAXS patterns of neat films of a) H-BDF-T, b) Cl-BDF-T, c) H-BDF-F, d) Cl-BDF-F, e) H-BDF-A, f) Cl-BDF-A.

further supported by recent results. For example, when T is used as a comonomer in thienoisatin-based BDF-copolymers, a mixed face-on/edge-on orientation is found along with an improvement in electrical conductivity. If, however, bithiophene and vinylene comonomers are used, linear backbones are obtained, leading to edge-on orientations and lower conductivities.[40] Completely linear backbones may, in turn, not allow for the intercalation of the dopant molecules and hence efficient doping at high MR. Instead, the curved backbones of the T-copolymers H-BDF-T and Cl-BDF-T allow for better doping efficiency but lead to less ordered packing at the same time, resulting in a somewhat reduced efficiency of interchain transport.

With doping, all copolymers retained their semicrystalline microstructure (see Figures S32–S37, Supporting Information) with only minor changes. For example, H-BDF-F exhibited a small increase in the main chain side chain separation distance from ≈3.8 to ≈4.1 nm upon doping, along with a decrease in π–π stacking order (see Figure S36, Supporting Information). As these changes do not reflect the amount of N-DMBI blended into the film, it is reasonable to assume that the majority of the dopant is located in the amorphous polymer domains. Evidence of diffraction from a crystalline phase of DMBI is not seen even for the highest doping levels probed.

What can be further seen from the GIWAXS measurements is that the morphology of H-BDF-F is much better ordered compared to H-BDF-T. **Figure 7** shows the strong improvement in ordering upon exchanging T by F, with H-BDF-F showing multiple orders of the 100 reflection. This is consistent with the

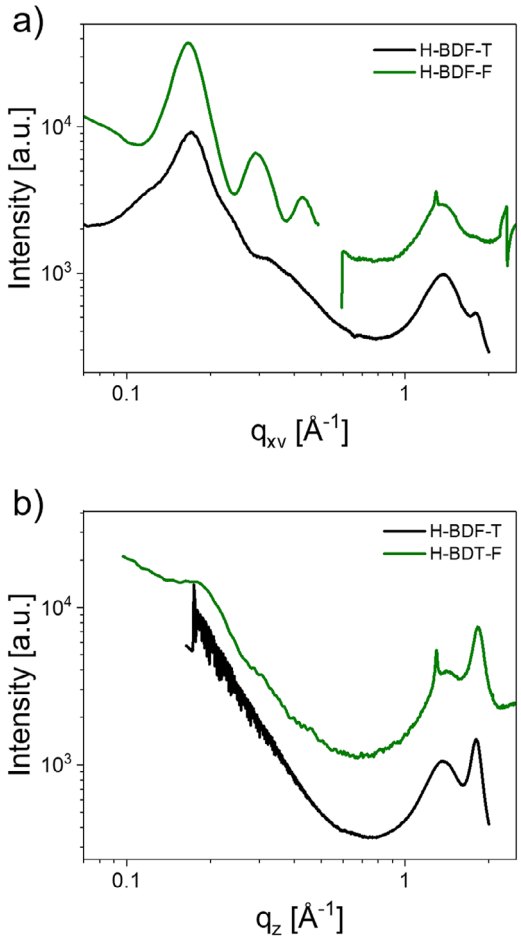

Figure 7. Comparison of the GIWAXS curves of H-BDF-T and H-BDF-F for in-plane a) and out-of-plane b) scattering directions.

enhanced coplanarity predicted in Scheme 2. In addition, a slight decrease in π–π-stacking distance is seen for H-BDF-F (3.44 Å) compared to H-BDF-T (3.49 Å), which again is a result of the improved coplanarity of H-BDF-F. These two aspects finally explain the high conductivity of this sample. The improvement in order together with the formation of face-on crystallites may also explain the slower and less strong decline of conductivity under ambient conditions, as oxygen diffusion in the vertical direction may be reduced.

3. Conclusion

Density functional theory (DFT) calculations were used as a starting point to establish structure-function relationships of BDF-isatin-comonomer conjugated copolymers for thermoelectric applications. Thiophene (T), furan (F), and acetylene (A) were considered as comonomers due to their varying geometries and ease of synthesis. Chlorination of the isatin motif was additionally considered due to easy synthetic realization and to stabilize the LUMO energy level of the backbones. The DFT calculations revealed that chlorination lowers the LUMO level by ≈0.2 eV in all cases compared to non-chlorinated analogues. The combined effects of chlorination and varying comonomers resulted in different levels of backbone torsion, conformation, and curvature. Non-chlorinated copolymers with T and F were calculated to have a mostly coplanar and wavy backbone structure that was preserved upon changing *syn*- and *anti*-conformations. In contrast, chlorination caused steric hindrance of *syn*-conformers, making coplanar *anti*-conformers more stable. However, the overall degree of coplanarity of chlorinated copolymers was lower, as the sum of conformations possible at room temperature is decisive for the backbone structure. Fully coplanar backbones were only possible for non-chlorinated A and F copolymers. Only A copolymer had a fully linear backbone structure. Experimentally, chlorination was achieved in a single step, and all copolymers were readily synthesized using short routes and Stille polymerization, furnishing six copolymers in good yields and molecular weights. Their LUMO energy levels were determined utilizing different techniques, including cyclic voltammetry and ultraviolet photoelectron / inverse photoelectron spectroscopy, showing good agreement with the results from DFT calculations and confirming chlorination to reduce the LUMO levels. The packing and crystallinity of the copolymers strongly depend on the comonomer and chlorination, with centrosymmetric A as comonomer showing crystalline packing and an exclusive edge-on orientation of the backbones. T and F copolymers both showed preferential face-on orientation, but the F copolymer exhibited a significantly increased degree of crystallinity as a result of the coplanar backbone structure. The combined effects of a curved, yet coplanar backbone structure, which led to face-on orientation and high crystallinity, overall endowed the non-chlorinated F copolymer with the highest electrical conductivity upon doping of these six copolymers. The fully linear, edge-on oriented A copolymers did not yield any measurable electrical conductivity. The resulting power factors were highest for the two copolymers with the highest conductivity, H-BDF-F and Cl-BDF-T, reaching power factor values of up to 0.2 μW m^{-1} K^{-2}. The small size of furan as a comonomer leads to a beneficial set of properties useful for thermoelectric applications.

4. Experimental Section

All details regarding starting materials, methods, synthesis of monomers and polymers, and their characterizations are given in the Supporting Information.

Supporting Information

Supporting Information is available from the Wiley Online Library or from the author.

Acknowledgements

This project has received funding from the European Union's Horizon 2020 research and innovation program under the Marie Skłodowska-Curie grant agreement No 955837 – HORATES. This research used the Soft Matter Interfaces (SMI) beamline (Beamline 12-ID) of the National Synchrotron Light Source II, a U.S. Department of Energy (DOE) Office of Science User Facility operated for the DOE Office of Science by the Brookhaven National Laboratory under contract no. DE-SC0012704. This work was also performed in part at the SAXS/WAXS beamline at the Australian Synchrotron, part of ANSTO. S.O. acknowledges funding from the

German Research Foundation (DFG) through a Heisenberg Professorship (project number OL 462/7-1). The authors thank Dr. Anders Mårtensson for SEC measurements. SO, KS, and KM acknowledge funding by the German Science Foundation (DFG) through the Research Training Group "Template-Designed Organic Electronics (TIDE)" (RTG-2591).

Conflict of Interest

The authors declare no conflict of interest.

Data Availability Statement

The data that support the findings of this study are available from the corresponding author upon reasonable request.

Keywords

backbone curvature, benzodifuranone, conjugated polymers, electrical conductivity, microstructure, organic thermoelectrics

Received: March 26, 2025
Revised: May 26, 2025
Published online: July 2, 2025

[1] K. Müllen, U. Scherf, *Macromol. Chem. Phys.* **2023**, *224*, 2200337.
[2] J. H. Burroughes, D. D. C. Bradley, A. R. Brown, R. N. Marks, K. Mackay, R. H. Friend, P. L. Burns, A. B. Holmes, *Nature* **1990**, *347*, 539.
[3] A. C. Grimsdale, K. Leok Chan, R. E. Martin, P. G. Jokisz, A. B. Holmes, *Chem. Rev.* **2009**, *109*, 897.
[4] G. Horowitz, *Adv. Mater.* **1998**, *10*, 365.
[5] H. Sirringhaus, *Adv. Mater.* **2014**, *26*, 1319.
[6] J. Yang, Z. Zhao, S. Wang, Y. Guo, Y. Liu, *Chem* **2018**, *4*, 2748.
[7] A. Facchetti, *Chem. Mater.* **2011**, *23*, 733.
[8] J. Yuan, Y. Zhang, L. Zhou, G. Zhang, H.-L. Yip, T.-K. Lau, X. Lu, C. Zhu, H. Peng, P. A. Johnson, M. Leclerc, Y. Cao, J. Ulanski, Y. Li, Y. Zou, *Joule* **2019**, *3*, 1140.
[9] B. Russ, A. Glaudell, J. J. Urban, M. L. Chabinyc, R. A. Segalman, *Nat. Rev. Mater.* **2016**, *1*, 16050.
[10] O. Bubnova, X. Crispin, *Energy Environ. Sci.* **2012**, *5*, 9345.
[11] L. Huang, N. Eedugurala, A. Benasco, S. Zhang, K. S. Mayer, D. J. Adams, B. Fowler, M. M. Lockart, M. Saghayezhian, H. Tahir, E. R. King, S. Morgan, M. K. Bowman, X. Gu, J. D. Azoulay, *Adv. Funct. Mater.* **2020**, *30*, 1909805.
[12] H. Cai, H. Tang, T. Wang, C. Xu, J. Xie, M. Fu, X. Luo, Z. Hu, Y. Zhang, Y. Deng, G. Li, C. Liu, F. Huang, Y. Cao, *Angew. Chem., Int. Ed.* **2024**, *63*, 202402375.
[13] T. L. D. Tam, C. K. Ng, S. L. Lim, E. Yildirim, J. Ko, W. L. Leong, S.-W. Yang, J. Xu, *Chem. Mater.* **2019**, *31*, 8543.
[14] D. T. Duong, C. Wang, E. Antono, M. F. Toney, A. Salleo, *Org. Electron.* **2013**, *14*, 1330.
[15] I. McCulloch, M. Heeney, M. L. Chabinyc, D. DeLongchamp, R. J. Kline, M. Cölle, W. Duffy, D. Fischer, D. Gundlach, B. Hamadani, R. Hamilton, L. Richter, A. Salleo, M. Shkunov, D. Sparrowe, S. Tierney, W. Zhang, *Adv. Mater.* **2009**, *21*, 1091.
[16] D.-D. Li, J.-X. Wang, Y. Ma, H.-S. Qian, D. Wang, L. Wang, G. Zhang, L. Qiu, Y.-C. Wang, X.-Z. Yang, *ACS Appl. Mater. Interfaces* **2016**, *8*, 19312.
[17] Y. Lu, Z. Yu, R. Zhang, Z. Yao, H. You, L. Jiang, H. Un, B. Dong, M. Xiong, J. Wang, J. Pei, *Angew. Chem., Int. Ed.* **2019**, *58*, 11390.
[18] K. Shi, F. Zhang, C.-A. Di, T.-W. Yan, Y. Zou, X. Zhou, D. Zhu, J.-Y. Wang, J. Pei, *J. Am. Chem. Soc.* **2015**, *137*, 6979.
[19] Y.-Z. Dai, N. Ai, Y. Lu, Y.-Q. Zheng, J.-H. Dou, K. Shi, T. Lei, J.-Y. Wang, J. Pei, *Chem. Sci.* **2016**, *7*, 5753.
[20] K. Feng, H. Guo, J. Wang, Y. Shi, Z. Wu, M. Su, X. Zhang, J. H. Son, H. Y. Woo, X. Guo, *J. Am. Chem. Soc.* **2021**, *143*, 1539.
[21] Z. Ji, Z. Li, L. Liu, Y. Zou, C. Di, D. Zhu, *Adv. Mater. Technol.* **2024**, *9*, 2302128.
[22] A. W. Van Herwaarden, P. M. Sarro, *Sens. Actuators* **1986**, *10*, 321.
[23] X. Rodríguez-Martínez, F. Saiz, B. Dörling, S. Marina, J. Guo, K. Xu, H. Chen, J. Martin, I. McCulloch, R. Rurali, J. S. Reparaz, M. Campoy-Quiles, *Adv. Energy Mater.* **2024**, *14*, 2401705.
[24] W. Zhao, J. Ding, Y. Zou, C. Di, D. Zhu, *Chem. Soc. Rev.* **2020**, *49*, 7210.
[25] F. Pallini, S. Mattiello, N. Manfredi, S. Mecca, A. Fedorov, M. Sassi, K. Al Kurdi, Y.-F. Ding, C.-K. Pan, J. Pei, S. Barlow, S. R. Marder, T.-Q. Nguyen, L. Beverina, *J. Mater. Chem. A* **2023**, *11*, 8192.
[26] D. Kiefer, R. Kroon, A. I. Hofmann, H. Sun, X. Liu, A. Giovannitti, D. Stegerer, A. Cano, J. Hynynen, L. Yu, Y. Zhang, D. Nai, T. F. Harrelson, M. Sommer, A. J. Moulé, M. Kemerink, S. R. Marder, I. McCulloch, M. Fahlman, S. Fabiano, C. Müller, *Nat. Mater.* **2019**, *18*, 149.
[27] S. Griggs, A. Marks, H. Bristow, I. McCulloch, *J. Mater. Chem. C* **2021**, *9*, 8099.
[28] H. Tang, Y. Liang, C. Liu, Z. Hu, Y. Deng, H. Guo, Z. Yu, A. Song, H. Zhao, D. Zhao, Y. Zhang, X. Guo, J. Pei, Y. Ma, Y. Cao, F. Huang, *Nature* **2022**, *611*, 271.
[29] I. Salzmann, G. Heimel, M. Oehzelt, S. Winkler, N. Koch, *Acc. Chem. Res.* **2016**, *49*, 370.
[30] A. D. Scaccabarozzi, A. Basu, F. Aniés, J. Liu, O. Zapata-Arteaga, R. Warren, Y. Firdaus, M. I. Nugraha, Y. Lin, M. Campoy-Quiles, N. Koch, C. Müller, L. Tsetseris, M. Heeney, T. D. Anthopoulos, *Chem. Rev.* **2022**, *122*, 4420.
[31] D. Kiefer, A. Giovannitti, H. Sun, T. Biskup, A. Hofmann, M. Koopmans, C. Cendra, S. Weber, L. J. Anton Koster, E. Olsson, J. Rivnay, S. Fabiano, I. McCulloch, C. Müller, *ACS Energy Lett.* **2018**, *3*, 278.
[32] Y. Shin, M. Massetti, H. Komber, T. Biskup, D. Nava, G. Lanzani, M. Caironi, M. Sommer, *Adv. Electron. Mater.* **2018**, *4*, 1700581.
[33] C.-Y. Yang, Y.-F. Ding, D. Huang, J. Wang, Z.-F. Yao, C.-X. Huang, Y. Lu, H.-I. Un, F.-D. Zhuang, J.-H. Dou, C. Di, D. Zhu, J.-Y. Wang, T. Lei, J. Pei, *Nat. Commun.* **2020**, *11*, 3292.
[34] I. E. Jacobs, A. J. Moulé, *Adv. Mater.* **2017**, *29*, 1703063.
[35] X. Wang, Z. Yu, Y. Lu, Z. Yao, Y. Zhou, C. Pan, Y. Liu, Z. Wang, Y. Ding, J. Wang, J. Pei, *Adv. Mater.* **2023**, *35*, 2300634.
[36] H. Li, G. Ye, Y. Kuang, M. Ma, S. Shao, J. Liu, *Mater. Horiz.* **2025**, https://doi.org/10.1039/D5MH00067J.
[37] M. Ma, G. Ye, S. Jang, Y. Kuang, L. Zhang, S. Shao, L. J. A. Koster, D. Baran, J. Liu, *ACS Energy Lett.* **2025**, *10*, 1813.
[38] S. Wang, H. Sun, U. Ail, M. Vagin, P. O. Å. Persson, J. W. Andreasen, W. Thiel, M. Berggren, X. Crispin, D. Fazzi, S. Fabiano, *Adv. Mater.* **2016**, *28*, 10764.
[39] T. Lei, Y. Cao, X. Zhou, Y. Peng, J. Bian, J. Pei, *Chem. Mater.* **2012**, *24*, 1762.
[40] Y. Lu, Z. Yu, H. Un, Z. Yao, H. You, W. Jin, L. Li, Z. Wang, B. Dong, S. Barlow, E. Longhi, C. Di, D. Zhu, J. Wang, C. Silva, S. R. Marder, J. Pei, *Adv. Mater.* **2021**, *33*, 2005946.
[41] D. R. Hinojosa, N. J. Pataki, P. Rossi, A. Erhardt, S. Guchait, F. Pallini, C. McNeill, C. Müller, M. Caironi, M. Sommer, *ACS. Appl. Polym. Mater.* **2024**, *6*, 457.
[42] R. Matsidik, A. Luzio, Ö. Askin, D. Fazzi, A. Sepe, U. Steiner, H. Komber, M. Caironi, M. Sommer, *Chem. Mater.* **2017**, *29*, 5473.
[43] T. Lei, J.-H. Dou, X.-Y. Cao, J.-Y. Wang, J. Pei, *J. Am. Chem. Soc.* **2013**, *135*, 12168.
[44] Z. Bao, W. K. Chan, L. Yu, *J. Am. Chem. Soc.* **1995**, *117*, 12426.

[45] T. Lei, X. Xia, J.-Y. Wang, C.-J. Liu, J. Pei, *J. Am. Chem. Soc.* **2014**, *136*, 2135.
[46] Z.-Y. Wang, Z.-F. Yao, Y. Lu, L. Ding, Z.-D. Yu, H.-Y. You, X.-Y. Wang, Y.-Y. Zhou, L. Zou, J.-Y. Wang, J. Pei, *Polym. Chem.* **2020**, *11*, 3716.
[47] M. E. Ziffer, S. B. Jo, Y. Liu, H. Zhong, J. C. Mohammed, J. S. Harrison, A. K.-Y. Jen, D. S. Ginger, *J. Phys. Chem. C* **2018**, *122*, 18860.
[48] C. M. Cardona, W. Li, A. E. Kaifer, D. Stockdale, G. C. Bazan, *Adv. Mater.* **2011**, *23*, 2367.
[49] D. Scheunemann, E. Järsvall, J. Liu, D. Beretta, S. Fabiano, M. Caironi, M. Kemerink, C. Müller, *Chem. Phys. Rev.* **2022**, *3*, 021309.
[50] X. Zhan, A. Facchetti, S. Barlow, T. J. Marks, M. A. Ratner, M. R. Wasielewski, S. R. Marder, *Adv. Mater.* **2011**, *23*, 268.
[51] S. B. Schmidt, M. Hönig, Y. Shin, M. Cassinelli, A. Perinot, M. Caironi, X. Jiao, C. R. McNeill, D. Fazzi, T. Biskup, M. Sommer, *ACS Appl. Polym. Mater.* **2020**, *2*, 1954.
[52] Y. W. Soon, S. Shoaee, R. S. Ashraf, H. Bronstein, B. C. Schroeder, W. Zhang, Z. Fei, M. Heeney, I. McCulloch, J. R. Durrant, *Adv. Funct. Mater.* **2014**, *24*, 1474.